PNAS RESEARCH ARTICLE | PHYSICS OPEN ACCESS

Quantum spin liquid from electron–phonon coupling

Xun Cai[a], Zhaoyu Han[b], Zi-Xiang Li[a,1], Steven A. Kivelson[b,1], and Hong Yao[c,1]

Contributed by Steven Kivelson; received December 12, 2024; accepted June 18, 2025; reviewed by David A. Huse, Patrick A. Lee, and Michael P. Zaletel

A quantum spin liquid (QSL) is an exotic insulating phase with emergent gauge fields and fractionalized excitations. However, the unambiguous demonstration of the existence of a QSL in a "nonengineered" microscopic model (or in any material) remains challenging. Here, using numerically exact sign-problem-free quantum Monte Carlo simulations, we show that a QSL arises in a nonengineered electron–phonon model. Specifically, we investigate the ground-state phase diagram of the bond Su–Schrieffer–Heeger model on a 2D triangular lattice at (one electron per site), which we show includes a QSL phase which is fully gapped, exhibits no symmetry-breaking order, and supports deconfined fractionalized holon excitations. This suggests promising routes for finding QSLs in realistic materials and high-T_c superconductivity by lightly doping them.

quantum spin liquids | electron–phonon coupling | quantum Monte Carlo

Significance

The search for quantum spin liquids—an exotic phase of matter that features fractionalization and topological order—has primarily focused on frustrated antiferromagnets. In this work, we reveal an alternative route to its physical realization in systems with strong coupling of electrons to relatively high-frequency phonons. We obtained unambiguous numerical evidence of this phase from large-scale sign-free quantum Monte Carlo simulations of a simple and physical model on a triangular lattice.

One of the central focuses of modern condensed matter physics has been the quest for a physical system with a quantum spin liquid (QSL) ground state (1), an exotic insulating state harboring fractionalized excitations, deconfined emergent gauge fields, and topological order. (For reviews, see, e.g., refs. 2–10.) Research on QSLs has been largely motivated by their intriguing properties such as fractionalized excitations, potential relevance to high-T_c superconductivity (SC) (11–14), and their potential applications in topological quantum computation (15, 16). Despite tremendous experimental efforts in the past decades (see, e.g., refs. 17–27), *unambiguous* experimental evidence establishing the existence of a QSL in any real material remains elusive. Consequently, analytically or numerically exact solutions of "natural" or "nonengineered" microscopic models that establish the existence of a QSL phase are of fundamental importance and can potentially provide useful guidance in searching for QSLs in realizable materials.

To date, most analytical and numerical studies have been devoted to searching for QSLs in frustrated quantum magnets where only local repulsion between electrons are considered (see e.g., refs. 28–66). Since electron–phonon coupling (EPC) is also ubiquitous in materials, it is natural to ask (12) if EPC can be the primary microscopic mechanism of QSL formation. Nonetheless, exploration of QSLs induced by pure EPC has been rare partly because EPC generates attractions which tend to favor pairing between itinerant electrons instead of spin interactions between local magnetic moments. A recent development is the establishment of resonating-valence-bond (RVB) states from strong-coupling analyses of two special electron-phonon models defined on a (generalized) Lieb lattice (67, 68). Moreover, it was recently shown that a Su–Schrieffer–Heeger (SSH) type EPC on the *bipartite* square lattice can induce antiferromagnetic (AF) ordering as well as valence bond solid (VBS) phases (69–73), which partly motivates us to ask whether this type of EPC can induce a QSL on a *nonbipartite* lattice.

Here, we show that a QSL can indeed be found in such a nonengineered EPC model on the triangular lattice in a broad, intermediate coupling parameter regime. Specifically, we investigated a prototypical microscopic model featuring an SSH-type coupling between optical phonons and electrons on a triangular lattice. This model is sign-problem-free (74–79), so we have been able to study it using large-scale numerically exact determinant quantum Monte Carlo (QMC) simulations (80–83). The ground-state phase diagram inferred from the state-of-the-art QMC is shown in Fig. 1: The ground state possesses s-wave SC long-range order at weak EPC or whenever the phonon frequency is sufficiently high. VBS order is dominant for intermediate to strong EPC whenever the phonon frequency is sufficiently small.

Most significantly, a gapped QSL phase emerges between the SC and VBS phases. Several features accessible to large-scale QMC simulations are used to establish this: 1) The QSL has a finite gap to all excitations. 2) There are no spontaneously broken symmetries—at least none with an order parameter magnitude large enough to be detectable. 3) There exists a deconfined (fractionalized) holon excitation that has charge e and no spin. (Modulo only the possibility that we could be fooled were the confinement scale larger

Author affiliations: [a]Beijing National Laboratory for Condensed Matter Physics, Institute of Physics, Chinese Academy of Sciences, Beijing 100190, China; [b]Department of Physics, Stanford University, Stanford, CA 94305; and [c]Institute for Advanced Study, Tsinghua University, Beijing 100084, China

Author contributions: X.C., Z.H., Z.-X.L., S.A.K., and H.Y. designed research; performed research; and wrote the paper.

Reviewers: D.A.H., Princeton University; P.A.L., Massachusetts Institute of Technology; and M.P.Z., University of California Berkeley.

The authors declare no competing interest.

[1]To whom correspondence may be addressed. Email: zixiangli@iphy.ac.cn, kivelson@stanford.edu, or yaohong@tsinghua.edu.cn.

This article contains supporting information online at https://www.pnas.org/lookup/suppl/doi:10.1073/pnas.2426111122/-/DCSupplemental.

Published August 11, 2025.

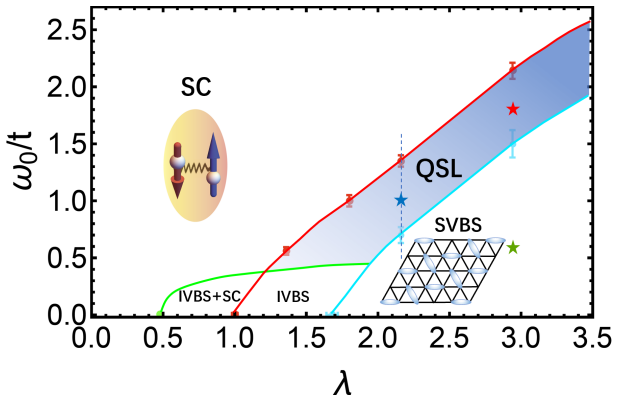

Fig. 1. Zero-temperature phase diagram of the SSH electron-phonon model at half-filling on triangular lattice with varying EPC strength λ and phonon frequency ω_0, obtained from state-of-the-art QMC simulations. Here, SC, SVBS, IVBS, and QSL denote s-wave superconductivity, staggered VBS, incommensurate VBS, and quantum spin liquid, respectively. The QSL to SC transition is shown to be continuous and consistent with XY* universality. The red and blue stars indicate the values of the parameters adopted for the calculations reported in Fig. 3 to establish that holons are deconfined/confined in the QSL and SVBS phases, respectively.

than our system sizes, this constitutes smoking-gun evidence (30) that the indicated phase is a QSL.) 4) We observe anomalous power-law correlations at the apparently continuous quantum phase transition between the QSL and SC phases, which is consistent with the XY* universality, expected (84) in this circumstance. We, moreover, provide a heuristic understanding of the emergence of QSL phases in this model employing a strong-coupling perspective. Our results unveil the emergence of a QSL in a nonengineered EPC model, an occurrence that, to the best of our knowledge, has not been previously reported.

The present results should serve as an inspiration to substantially broaden the search for QSL candidate materials—to include materials without any obvious magnetism but with strong EPC involving relatively high-frequency phonons, especially in cases in which the electronic bands are relatively flat. The proximity of the QSL to an SC phase is also suggestive that high-T_c SC might occur in proximity to such a QSL phase.

Model. We consider the bond SSH model on a triangular lattice described by the Hamiltonian:

$$\hat{H} = \sum_{\langle ij \rangle} \Big[-\left(t + g\hat{X}_{ij}\right)\hat{B}_{ij} + \frac{\hat{P}_{ij}^2}{2M} + \frac{K}{2}\hat{X}_{ij}^2 \Big], \quad [1]$$

where $\hat{B}_{ij} = \sum_\sigma (c_{i\sigma}^\dagger c_{j\sigma} + \text{h.c.})$ is the bond-density operator in which $c_{i\sigma}^\dagger$ creates an electron on site i with spin polarization $\sigma = \uparrow, \downarrow$, and $\hat{X}_{ij}$ and $\hat{P}_{ij}$ are, respectively, the displacement and momentum operators of an optical phonon residing on the bond between nearest-neighbor (NN) sites $\langle ij \rangle$. Here, t is the bare nearest-neighbor (NN) hopping amplitude and g is the EPC strength. The relevant dimensionless measure of the EPC strength is $\lambda \equiv \frac{zg^2}{KW}$, where $z = 6$ is the number of nearest-neighbors and $W = 9t$ is the electron's bare bandwidth on triangular lattice (85). For simplicity we have assumed Einstein phonons with bare frequency $\omega_0 = \sqrt{K/M}$. We set $\hbar = 1$ throughout this paper.

Because this model is free from the notorious fermion minus sign problem, we have been able to perform numerically exact QMC simulations to access the ground-state (zero-temperature) properties up to system sizes 18×18. To do this, we implemented projective determinant QMC simulations (86). We have focused on the model at half-filling by fixing the electron number rather than the chemical potential. The DQMC simulations on the model with strong electron–phonon coupling are typically computationally more demanding than purely electronic models due to the longer autocorrelation times. We have adopted various strategies to reduce the autocorrelation time; nonetheless heavy computational resources have still been required to achieve reliable results with high accuracy (details are in *SI Appendix*).

Ground-State Phase Diagram. The ground-state phase diagram in the extreme adiabatic limit, $\omega_0 = 0$, is shown along the *Bottom* line of Fig. 1. In this limit, quantum fluctuations of the phonon fields vanish and the phonon configurations $\{X_{ij}\}$ are static, so ground-state properties can be accessed straightforwardly by finding the phonon configurations $\{X_{ij}\}$ that minimize the adiabatic energy. For small λ, because the Fermi surface is not perfectly nested, a symmetry-preserving metallic ground-state is stable for λ smaller than a finite critical value. For stronger coupling, incommensurate VBS (IVBS) long-range order is found for $\lambda_{c1} < \lambda < \lambda_{c2}$ ($\lambda_{c1} \approx 0.42$ and $\lambda_{c2} \approx 1.62$) with a λ-dependent ordering vector that is not far from the optimal Fermi surface nesting vector. Even in the presence of IVBS order, ungapped pockets of Fermi surface persist for $\lambda_{c1} < \lambda < \lambda_{FS}$ ($\lambda_{FS} \approx 0.96$), while the fermionic spectrum is fully gapped for $\lambda_{FS} < \lambda < \lambda_{c2}$. In stronger coupling, $\lambda > \lambda_{c2}$, commensurate VBS order emerges with the staggered pattern shown in the *Inset* of Fig. 1. The transitions at λ_{c1} and λ_{FS} are continuous while the transition at λ_{c2} is first order, accompanied by a discontinuous jump in the ordering vector. (See *SI Appendix* for details.)

The phase diagram for small but nonzero ω_0 is readily inferred by continuity from $\omega_0 = 0$, as we have verified for finite ω_0 using QMC. Specifically, VBS persists to nonzero ω_0. Moreover, with or without VBS order, the presence of a Fermi surface at $\omega_0 = 0$ for all $\lambda < \lambda_{FS}$ implies the existence of a Cooper instability and hence the emergence of superconducting order at small but nonzero ω_0 - an expectation that is consistent with our QMC results in the studied range $\omega_0/t \gtrsim 0.5$. In the regime close to the onset of IVBS order, SC should coexist with IVBS. Generally, the SC phase expands and the VBS phases are pushed to higher λ with increasing ω_0. Most significantly, in an intermediate regime of ω_0 and λ, we find a fully gapped Z_2 QSL in the ground state.

Broken Symmetries. To determine where in the phase diagram the ground-state has various patterns of spontaneous symmetry-breaking, we have computed the structure factor $S(\boldsymbol{q}, L) = \frac{1}{L^4}\sum_{ij} e^{i\boldsymbol{q}\cdot(\boldsymbol{r}_i - \boldsymbol{r}_j)}\langle \hat{O}_i^\dagger \hat{O}_j \rangle$ and the associated correlation-length ratio

$$R^c(L) \equiv 1 - \frac{S(\boldsymbol{Q} + \delta\boldsymbol{q}, L)}{S(\boldsymbol{Q}, L)} \to \begin{cases} 1 \\ |\delta q\, \xi|^2 \end{cases}, \quad [2]$$

where $\hat{O}_j$ is one of a number of possible local order-parameter fields, $\boldsymbol{Q}$ is the momentum at which the structure factor peaks and $|\delta\boldsymbol{q}| = 4\pi/\sqrt{3}L$ is the minimum crystalline momentum on a lattice with system size $L \times L$. As indicated in the equations, in a broken symmetry phase, $S(\boldsymbol{Q}, L) \to |\Phi|^2$ and $R^c(L) \to 1$ as $L \to \infty$, where $|\Phi|$ is the magnitude of the order parameter, while with only short-range order, it follows that $S(\boldsymbol{Q}, L) \to 0$ and that $R^c(L) \sim (\xi/L)^2 \to 0$ as $L \to \infty$, where ξ is the correlation length. As a function of a control parameter, a

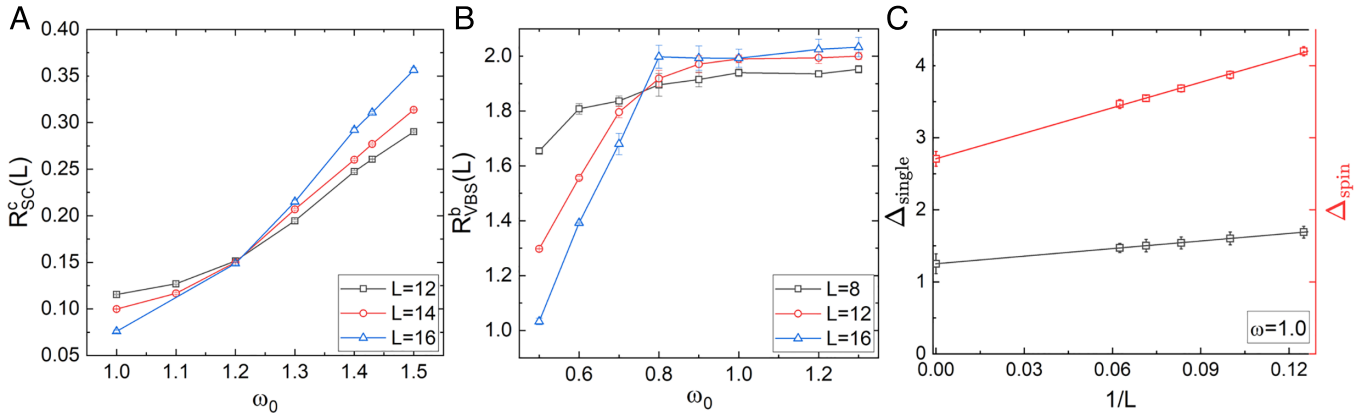

Fig. 2. QMC results on the triangular lattice with size $L \times L$, where the EPC strength is fixed at $\lambda = 2.16$ (corresponding to $g = 1.8$). (*A*) The correlation-length ratio (defined in Eq. **2**) for onsite s-wave superconducting order as a function of ω_0. The crossing point for different system sizes indicates that the transition between the SC and non-SC (QSL) phases occurs at $\omega_0 \approx 1.2$. (*B*) The Binder ratio (defined in *SI Appendix*, Eq. **S5**) for SVBS order as a function of ω_0. The transition between SVBS and the uniform (QSL) phase occurs at $\omega_0 \approx 0.7$. (*C*) Finite-size-scaling results of the single-particle and spin gaps, Δ_{single} and Δ_{spin}, in the QSL phase for $\omega_0 = 1.0$. Both Δ_{single} and Δ_{spin} extrapolate to finite values as $L \to \infty$, confirming the fully gapped character of the QSL phase.

symmetry-breaking transition can be identified, as in Fig. 2*A*, with a crossing point at which $R^c(L)$ transitions from being a decreasing to an increasing function of L, i.e., a point at which $R^c(L)$ is independent of L for large L. We also consider the Binder ratio $R^b(L)$ to identify the phase transition to a state with spontaneous symmetry breaking, as shown in Fig. 2*B*. Details of correlation-length and Binder ratios are in *SI Appendix*.

An example of this analysis is shown in Fig. 2, where for a fixed value of $\lambda = 2.16$ (corresponding to $g = 1.8$) we have computed the superconductivity correlation-length ratio R^c_{SC} (i.e. with $\hat{O}_i$ corresponding to an onsite s-wave pair-field creation operator $c_{i\uparrow}c_{i\downarrow}$ and $\boldsymbol{Q} = \boldsymbol{0}$) and the staggered VBS Binder ratio R^b_{VBS} [i.e. with O_i corresponding to a valence bond density operator and $\boldsymbol{Q} = (\pi, 0)$] as a function of ω_0 for L up to $L = 16$. The SC correlation-length ratio $R^c_{SC}(L)$ (shown in Fig. 2*A*) increases with system size when $\omega_0 \geq 1.2$, indicating that the ground state possesses long-ranged SC order, and decreases for $\omega_0 < 1.2$, implying only short-range SC correlations. At sufficiently low frequency $\omega_0 < 0.7$, the order in the ground state is a staggered VBS, as evidenced by the results of VBS Binder ratios (shown in Fig. 2*B*). Consequently, in the intermediate frequency regime $0.7 < \omega_0 < 1.2$, the ground state has neither SC nor VBS order. We have repeated the same analysis for $\lambda = 2.94$ (i.e. $g = 2.1$), and again found an intermediate range of ω_0 with neither SC nor VBS ordering, as shown in Fig. 1. We further checked for and found no evidence indicating other possible spontaneously broken symmetries in the intermediate phase, including other forms of VBS ordering (other values of $\boldsymbol{Q}$) such as columnar VBS and $\sqrt{12} \times \sqrt{12}$ plaquette VBS, and loop current ordering (details are included in *SI Appendix*). Thus, there apparently exists, in a range of intermediate λ and ω_0, a symmetric phase without any spontaneous symmetry breaking, consistent with a QSL phase.

Spectral Features of the QSL. We have also obtained information concerning the single-particle and neutral spin spectra by analyzing the corresponding imaginary-time correlators in the intermediate phase with no symmetry breaking order. In both cases, we find that the local two-time correlator falls exponentially with time, implying a gap in the spectrum. (Details of the fitting procedure are presented in *SI Appendix*.) The single-particle and spin gap inferred in this way for representative couplings, $\lambda = 2.16$ and $\omega_0 = 1.0$, in the intermediate phase are shown for various system sizes, L, in Fig. 2*C*, from which it is apparent that they both extrapolate to a finite value in the limit $L \to \infty$. The bond–bond correlations obtained from QMC are short-ranged with a short correlation length (less than one lattice constant); the singlet gap is smaller but also finite (see *SI Appendix* for details). Consequently, the symmetric intermediate phase is fully gapped. According to the celebrated Lieb-Schultz-Mattis-Oshikawa-Hastings theorem (87–89), any symmetric phase with a finite excitation gap on a triangular lattice at half-filling of spin-$\frac{1}{2}$ electrons cannot be a trivial phase; it must be a gapped QSL with accompanying topological order.

Fractionalized Excitations. To corroborate its existence, it is desirable to establish direct signatures of a QSL, for instance, the existence of fractionalized excitations such as deconfined holons. The energy cost of creating two spatially separated holons in a QSL approaches a finite constant even when they are far from each other. In contrast, in any topologically trivial phase such as a VBS, holons are confined in the sense that the energy cost of creating two far separated holons increases linearly with separation. (Since the spin gap is finite, the energy cost of two far-separated e charges in a confining phase ceases to grow linearly beyond a critical separation determined by the spin-gap. For larger separations, it is energetically favorable to create two accompanying charge 0 spin 1/2 "spinons," so that the charge excitations become a pair of ordinary charge e spin 1/2 holes.)

To investigate holon deconfinement, we perform QMC simulations for the same model but with two electrons (with opposite S^z) removed from the half-filled system. Moreover, we localize the associated excitations by adding two "impurity" potentials to the Hamiltonian,

$$\hat{H} \to \hat{H} + \sum_{\alpha=1,2} V_p \hat{n}_{\vec{r}_\alpha} \qquad [3]$$

which couple to the local charge (relative to half-filling) at two separate sites $\vec{r}_1$ and $\vec{r}_2$, respectively, as schematically shown as red points in the *Inset* of Fig. 3*A*. Simulations have been performed on lattices of size $L_x \times L_y$, with $L_y = 8$, and with the two impurity sites separated in the x direction by $r_{12} = |\vec{r}_1 - \vec{r}_2| = L_x/2$. We

focus particularly on the energy difference between doped systems with and without impurity potential V, and the two-point correlations $\langle \hat{Q}_1 \hat{Q}_2 \rangle$ and $\langle \hat{\mathcal{S}}_1^z \hat{\mathcal{S}}_2^z \rangle$, where $\hat{Q}_\alpha \equiv \sum_{i \in R_\alpha} (\hat{n}_i - 1)$ and z-component of spin, $\hat{\mathcal{S}}_\alpha^z \equiv \sum_{i \in R_\alpha} \hat{S}_i^z$ in each of two spatially separated regions R_α (R_α consisting of the site $\vec{r}_\alpha$ and its first and second neighbors, as illustrated by the circles in the *Inset* of Fig. 3*A*) for different values of L_x. The on-site impurity potential is fixed at $V_p = 30$.

The results of charge and spin correlations are shown in Fig. 3 *A* and *B*, respectively. In the QSL regime, with increasing L_x the charge correlation grows to a value close to one, while the spin correlation vanishes, implying that the excitation trapped by each impurity potential is a holon with charge-*e* but spin-zero. The energy difference ΔE between the states of the doped holes with and without impurity potentials is shown in Fig. 3*C*; ΔE approximately saturates to a constant for $r_{12} \geq 6$, as expected for deconfined holons. For comparison, we performed similar calculations in the regime of VBS. The behaviors of charge and spin correlations in the VBS phase are qualitatively similar to those in the QSL regime, as presented in Fig. 3 *A* and *B*, implying that the excitations trapped by impurity potentials in the VBS are also holons; however, the energy cost ΔE increases roughly linearly with r_{12}, as expected in a (weakly) confining phase. The results are consistent with the expectation of deconfined holons only in the QSL phase.

It is in principle possible for the holons to be fermionic or bosonic—a feature determined by energetics rather than by the topology of the state (90). This could ideally be measured by determining the adiabatic phase under exchange, but this is not possible with our present approach (91). However, the fact that the QSL to SC phase transition (see below) is consistent with condensation of bosonic holons (30, 84) suggests that the holons are bosonic.

Quantum Phase Transitions. Although the QSL phase is fully gapped, on approach to any continuous transition from this to another phase, one or more gaps are expected to vanish. (If the transition is, instead, weakly first order, the appropriate gap should get small but not quite vanish—a subtle distinction that we might not be able to distinguish without more extensive studies than we have so far carried out.) Given that the QSL to SC transition appears to be continuous, we would expect the spin and quasiparticle gaps to remain finite at and on both sides of the transition, but the charge gap should vanish at the transition and in the SC phase. As shown in *SI Appendix*, Fig. S7, we have verified that indeed the charge gap vanishes at two representative points, one on the QSL-SC phase boundary and one in the SC phase, while the single-particle and spin gaps are nonzero. At a continuous QSL to VBS transition, the spin, quasi-particle, and charge gaps should remain finite at and on both sides of the transition, but the gap to spin 0 neutral excitations—which is finite in both phases—should vanish at the transition. We have not explicitly tested this at present.

The quantum phase transition between the insulating state and the neighboring SC phase is expected to exhibit additional distinct features if the insulating phase supports fractionalized excitations. Specifically, the quantum phase transition from a QSL with Z_2 topological order to a conventional (s-wave) SC can proceed through the condensation of holons/doublons ("chargeons"); the corresponding critical properties (84) are characterized by 3d XY* universality, reflecting the existence of fractionalized excitations and exhibiting power-law correlations at criticality with a very large anomalous dimension $\eta_{XY^*} \approx 1.49$ (92). In contrast, the transition between a conventional insulator and an SC, or between a QSL and an exotic SC* phase (with deconfined visons) is expected to exhibit conventional 3d XY criticality, i.e. with $\eta_{XY} \approx 0.034$. By numerical analysis of pair–pair correlations at the QSL-SC transition in the present model, as detailed in *SI Appendix*, we found a $\eta \approx 1.45 \pm 0.08$, consistent with an XY* transition within the error bar. This further confirms that the symmetry-preserving insulating phase in the triangular SSH model is a Z_2 QSL.

Strong Coupling Analysis. We can get a feeling for why a QSL phase arises and what its character is, by approaching the problem from the theoretically tractable strong coupling limit, where $t \ll g^2/K$ (i.e. $\lambda \gg 1$) and $\omega_0 \ll g^2/K$.

In the adiabatic limit $\omega_0 = 0$, complete identification of the degenerate ground-states can be obtained straightforwardly from a combination of analytic analysis and numerical solution of large finite size systems; the electronic Hamiltonian is noninteracting,

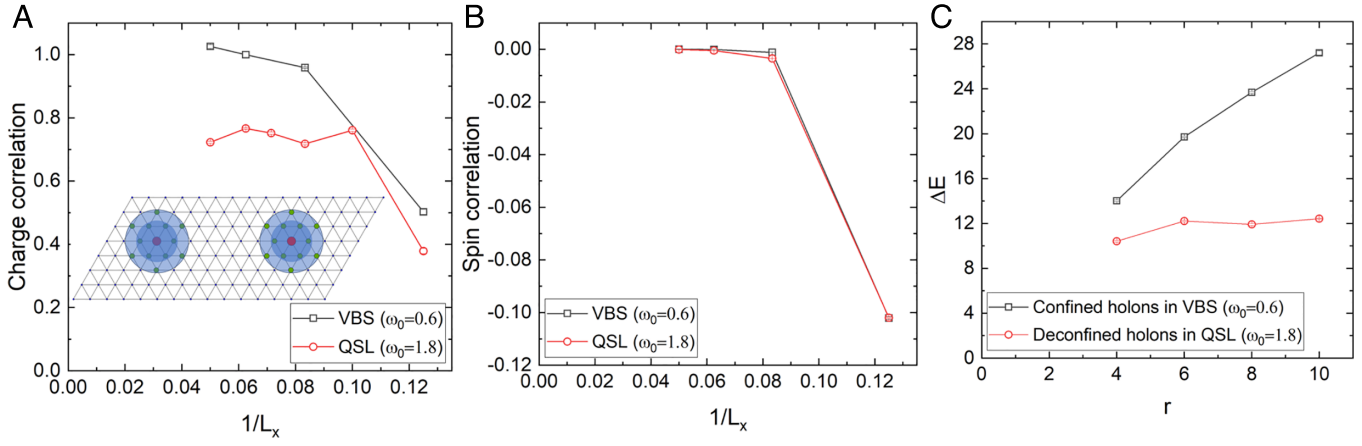

Fig. 3. QMC results for two holes doped away from half filling in terms of quantities defined in Eq. **3** and the following paragraph. The doped holes are localized in the neighborhood of two "impurities," $\alpha = 1$ & 2 as indicated by the red dots in the *Inset* of (*A*), on which there is an onsite potential $V_p = 30$; they are separated along the *x* direction by $r_{12} = L_x/2$. The EPC strength is fixed at $\lambda = 2.94$ and two representative values of ω_0 are treated: $\omega_0 = 0.6$ (in the SVBS) and $\omega_0 = 1.8$ (in the QSL). The interimpurity charge–charge ($\langle \hat{Q}_1 \hat{Q}_2 \rangle$) and spin–spin ($\langle \hat{S}_1^z \hat{S}_2^z \rangle$) correlations are shown as a function of $1/L_x$ in (*A* and *B*), respectively. The energy difference between the states with ($V_p = 30$) and without ($V_p = 0$) the impurity potential is shown in (*C*) as a function of r_{12}.

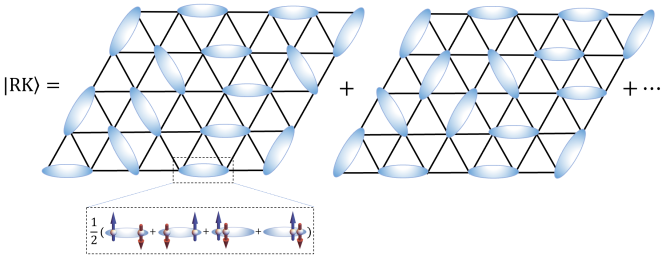

Fig. 4. A schematic representation of the RK wave function on the triangular lattice. Each dimer represents two electrons occupying the bonding orbital between two neighboring sites (see the dimer bond creation operator $b^{\dagger}_{\langle ij\rangle}$ after Eq. **4**).

so all that is required is to minimize the adiabatic energy with respect to the phonon coordinates, $\{X_{ij}\}$. Notably, to the first order in t, there is an extensive number of degenerate ground-states, which we will refer to as hard-core dimer states. They can be identified with fully packed configurations $\mathcal{C}$ of hard-core dimers, where each dimer labels a nearest-neighbor bond and where exactly one dimer touches each site of the lattice, as shown in Fig. 4. In the state $|\mathcal{C}\rangle$, two electrons occupy the bonding orbital on each dimer-covered bond so that the expectation value of $\langle \hat{B}_{ij}\rangle = 2$ and $\langle \hat{X}_{ij}\rangle = 2g/K$; on the remaining bonds, $\langle \hat{B}_{ij}\rangle = 0$ and $\langle \hat{X}_{ij}\rangle = 0$.

Restricting attention to the dimer states, we note that they remain degenerate with each other to first order in both t and ω_0.* To summarize, ignoring terms of higher than first order in t and ω_0, there is a manifold of degenerate ground states spanned by a set of linearly independent dimer states, $|\mathcal{C}\rangle$, in one-to-one correspondence with the set of hard-core dimer coverings of the lattice. The electron wavefunction of each state is

$$|\mathcal{C}\rangle_e = \prod_{\{ij\}\in C} \hat{b}^{\dagger}_{\langle ij\rangle}\,|\mathrm{vac}\rangle, \qquad [4]$$

where $\hat{b}^{\dagger}_{\langle ij\rangle} \equiv \frac{1}{2}(c^{\dagger}_{i\uparrow}+c^{\dagger}_{j\uparrow})(c^{\dagger}_{i\downarrow}+c^{\dagger}_{j\downarrow}) = \frac{1}{2}[(c^{\dagger}_{i\uparrow}c^{\dagger}_{j\downarrow}+c^{\dagger}_{j\uparrow}c^{\dagger}_{i\downarrow})+(c^{\dagger}_{i\uparrow}c^{\dagger}_{i\downarrow}+c^{\dagger}_{j\uparrow}c^{\dagger}_{j\downarrow})]$ is the valence bond creation operator and $|\mathrm{vac}\rangle$ is the empty state. The phonon wave functions are certain Gaussian states for the phonon modes with $\langle X_{ij}\rangle = 2g/K$ on occupied bonds and $\langle X_{ij}\rangle = 0$ on other bonds (details are given in *SI Appendix*).

Working in a higher order in t and ω_0, we could, in principle, obtain, in terms of the parameters of the original model, an effective model that operates in the hard-core dimer subspace. The form of the resulting effective hard-core quantum dimer Hamiltonian, $\hat{H}_{\mathrm{dimer}} = \hat{V}+\hat{J}$, is highly constrained, and indeed of precisely the same form as has been analyzed in various earlier studies in which the origin of the effective model is entirely different (30). There are two types of terms: interaction terms, $\hat{V}$, that are diagonal in the dimer basis, and kinetic terms, $\hat{J}$, that are off diagonal. To low order in the small parameters, both terms are short-range, so for convenience, we will explicitly consider only those involving pairs of nearest-neighbor dimers, i.e.

$$\hat{V} = V\sum_{\square}\left[\,|\,\rangle\langle\,|+|\,\rangle\langle\,|\,\right], \qquad [5]$$

where the thick lines represent dimers and the summation is over all possible four-sided plaquettes, and

$$\hat{J} = -J\sum_{\square}\left[\,|\,\rangle\langle\,|+|\,\rangle\langle\,|\,\right]. \qquad [6]$$

(Further range terms that are similar in structure occur as well, although they are still smaller than these most local terms in the strong-coupling limit.)

The interaction terms are relatively simple to compute. For instance, to second order in t and first order in ω_0, the interaction can be shown explicitly to be $V = t^2K/g^2 - \frac{\sqrt{2}-1}{2}\omega_0$ (details of derivations in *SI Appendix*). The kinetic term J necessarily vanishes for any t in the $\omega_0 \to 0$ limit as they are tunneling processes—akin to small bipolaron hopping—involving rearrangements of the phonon coordinates. For $0 < \omega_0 \ll t/\lambda$, where the potential energy still dominates the kinetic energy, the dimer repulsion ($V > 0$) favors a staggered VBS ground state, consistent with the results obtained from the large-scale QMC calculations for large values of λ and small ω_0/t. However, even if we restrict attention to the strong coupling limit, the distinct dependence of J and V on t and ω_0 implies that as a function of ω_0/t one can access the situation in which $J \approx V$, † in which case it has been shown that (on a nonbipartite lattice) there exists a perturbatively stable, gapped QSL phase with $\mathbb{Z}_2$ topological order (33, 49). In particular, at the special RK point (30), the ground state can be expressed as an equal superposition of all possible dimer covering configurations:

$$|\mathrm{RK}\rangle = \mathcal{N}^{-1/2}\sum_{\mathcal{C}}|\mathcal{C}\rangle, \qquad [7]$$

where $\mathcal{N}$ is the number of hard-core dimer states. A schematic representation of $|\mathrm{RK}\rangle$ is shown in Fig. 4. This is a short-range RVB state with $\mathbb{Z}_2$ topological order (15, 31–33), that we believe is a representative state of the QSL phase we demonstrated in the present QMC study.

Concluding Remarks. Using state-of-the-art QMC, we have established the existence of a QSL phase in the ground state of SSH electron-phonon models on a triangular lattice on the basis of multiple, independent criteria. This is a distinctive case for a nonengineered model, at least for one dominated by EPC. As SSH-type phonons exist commonly in quantum materials, our study points out a promising direction for the search for QSLs in systems, including twisted moire systems (93), with such phonon couplings.

As the SSH electron-phonon model in Eq. **1** is free from sign problems even for finite doping away from half-filling, its physical properties can be accurately studied by large-scale QMC simulations over a broader range of conditions, which is currently one of our ongoing efforts. In the near future, we intend to further explore the nature of the SC state proximate to the QSL to gain further insight into the nature of possible SC emerging from a lightly doped QSL (94–98), a problem that has been conjectured to have relevance to the cuprate superconductors (11–14).

*We have also verified the robustness of the nearly degenerate ground state manifold of the dimer states in the presence of various additional terms, e.g. onsite Hubbard repulsion and Holstein-type EPC.

†From the estimates of V and J as a function of t and ω_0 in the strong coupling limit, as shown in *SI Appendix*, one would conclude that $J \sim V$ only if $\omega_0 \sim t^2K/g^2$. Since the arguments we have presented so far rely not only on $\lambda \gg 1$, and $\omega_0K/g^2 \ll 1$, this requires us to extrapolate the strong coupling results to intermediate values of λ and ω_0K/g^2 to access the region studied by QMC. For this reason, the strong coupling analysis of the QSL phase just presented must be viewed as heuristic rather than controlled for the original EPC problem.

Data, Materials, and Software Availability. Some study data are available. The data files are huge. The relevant data are included in the manuscript. Upon request, within reason, we can provide more data to those who ask.

ACKNOWLEDGMENTS. We would like to thank Eduardo Fradkin, David Huse, Roger Melko, Subir Sachdev, T. Senthil, and Zhouquan Wan for helpful discussions; Z.H. and S.A.K. thank Kyung-Su Kim and John Sous for collaborations on related topics. This work was supported in part by the Ministry of Science & Technology of China under Grant No. 2021YFA1400100 (H.Y.), by National Natural Science Foundation of China under Grant Nos. 12347107 (X.C., Z.-X.L., and H.Y.) and 12334003 (H.Y.), by the New Cornerstone Science Foundation through the Xplorer Prize (H.Y.), and by NSF grant No. DMR-2310312 (Z.H. and S.A.K.).

1. P. Anderson, Resonating valence bonds: A new kind of insulator? *Mater. Res. Bull.* **8**, 153 (1973).
2. P. A. Lee, An end to the drought of quantum spin liquids. *Science* **321**, 1306–1307 (2008).
3. L. Balents, Spin liquids in frustrated magnets. *Nature* **464**, 199–208 (2010).
4. L. Savary, L. Balents, Quantum spin liquids: A review. *Rep. Prog. Phys.* **80**, 016502 (2016).
5. M. R. Norman, Colloquium: Herbertsmithite and the search for the quantum spin liquid. *Rev. Mod. Phys.* **88**, 041002 (2016).
6. X. G. Wen, Colloquium: Zoo of quantum-topological phases of matter. *Rev. Mod. Phys.* **89**, 041004 (2017).
7. Y. Zhou, K. Kanoda, T. K. Ng, Quantum spin liquid states. *Rev. Mod. Phys.* **89**, 025003 (2017).
8. J. Knolle, R. Moessner, A field guide to spin liquids. *Ann. Rev. Condens. Matter Phys.* **10**, 451–472 (2019).
9. C. Broholm *et al*., Quantum spin liquids. *Science* **367**, eaay0668 (2020).
10. S. A. Kivelson, S. Sondhi, 50 years of quantum spin liquids. *Nat. Rev. Phys.* **5**, 368–369 (2023).
11. P. W. Anderson, The resonating valence bond state in La_2CuO_4 and superconductivity. *Science* **235**, 1196–1198 (1987).
12. S. A. Kivelson, D. S. Rokhsar, J. P. Sethna, Topology of the resonating valence-bond state: Solitons and high-T_c superconductivity. *Phys. Rev. B* **35**, 8865–8868 (1987).
13. P. A. Lee, N. Nagaosa, X. G. Wen, Doping a Mott insulator: Physics of high-temperature superconductivity. *Rev. Mod. Phys.* **78**, 17–85 (2006).
14. P. W. Anderson *et al*., The physics behind high-temperature superconducting cuprates: The 'plain vanilla' version of RVB. *J. Phys. Condens. Matter* **16**, R755 (2004).
15. A. Kitaev, Fault-tolerant quantum computation by anyons. *Ann. Phys.* **303**, 2–30 (2003).
16. C. Nayak, S. H. Simon, A. Stern, M. Freedman, S. Das Sarma, Non-abelian anyons and topological quantum computation. *Rev. Mod. Phys.* **80**, 1083–1159 (2008).
17. Y. Okamoto, M. Nohara, H. Aruga-Katori, H. Takagi, Spin-liquid state in the $s = 1/2$ hyperkagome antiferromagnet $Na_4Ir_3O_8$. *Phys. Rev. Lett.* **99**, 137207 (2007).
18. M. Yamashita *et al*., Highly mobile gapless excitations in a two-dimensional candidate quantum spin liquid. *Science* **328**, 1246–1248 (2010).
19. F. L. Pratt *et al*., Magnetic and non-magnetic phases of a quantum spin liquid. *Nature* **471**, 612–616 (2011).
20. T. H. Han *et al*., Fractionalized excitations in the spin-liquid state of a Kagome-lattice antiferromagnet. *Nature* **492**, 406–410 (2012).
21. M. Fu, T. Imai, T. H. Han, Y. S. Lee, Evidence for a gapped spin-liquid ground state in a Kagome Heisenberg antiferromagnet. *Science* **350**, 655–658 (2015).
22. Y. Shen *et al*., Evidence for a spinon fermi surface in a triangular-lattice quantum-spin-liquid candidate. *Nature* **540**, 559–562 (2016).
23. A. Banerjee *et al*., Proximate Kitaev quantum spin liquid behaviour in a honeycomb magnet. *Nat. Mater.* **15**, 733–740 (2016).
24. A. Banerjee *et al*., Neutron scattering in the proximate quantum spin liquid α-$RuCl_3$. *Science* **356**, 1055–1059 (2017).
25. Y. Kasahara *et al*., Majorana quantization and half-integer thermal quantum hall effect in a Kitaev spin liquid. *Nature* **559**, 227–231 (2018).
26. B. Miksch *et al*., Gapped magnetic ground state in quantum spin liquid candidate κ-(BEDT-TTF)$_2$Cu$_2$(CN)$_3$. *Science* **372**, 276 (2021).
27. A. Scheie *et al*., Proximate spin liquid and fractionalization in the triangular antiferromagnet $KYbSe_2$. *Nat. Phys.* **20**, 74–81 (2024).
28. V. Kalmeyer, R. B. Laughlin, Equivalence of the resonating-valence-bond and fractional quantum hall states. *Phys. Rev. Lett.* **59**, 2095–2098 (1987).
29. G. Baskaran, Z. Zou, P. Anderson, The resonating valence bond state and high-T_c superconductivity - a mean field theory. *Solid State Commun.* **63**, 973–976 (1987).
30. D. S. Rokhsar, S. A. Kivelson, Superconductivity and the quantum hard-core dimer gas. *Phys. Rev. Lett.* **61**, 2376–2379 (1988).
31. N. Read, S. Sachdev, Large-n expansion for frustrated quantum antiferromagnets. *Phys. Rev. Lett.* **66**, 1773–1776 (1991).
32. X. G. Wen, Mean-field theory of spin-liquid states with finite energy gap and topological orders. *Phys. Rev. B* **44**, 2664–2672 (1991).
33. R. Moessner, S. L. Sondhi, Resonating valence bond phase in the triangular lattice quantum dimer model. *Phys. Rev. Lett.* **86**, 1881–1884 (2001).
34. L. Balents, M. P. A. Fisher, S. M. Girvin, Fractionalization in an easy-axis Kagome antiferromagnet. *Phys. Rev. B* **65**, 224412 (2002).
35. X. G. Wen, Quantum orders in an exact soluble model. *Phys. Rev. Lett.* **90**, 016803 (2003).
36. M. Hermele *et al*., Stability of $u(1)$ spin liquids in two dimensions. *Phys. Rev. B* **70**, 214437 (2004).
37. F. Wang, A. Vishwanath, Spin-liquid states on the triangular and Kagomé lattices: A projective-symmetry-group analysis of Schwinger boson states. *Phys. Rev. B* **74**, 174423 (2006).
38. A. Kitaev, Anyons in an exactly solved model and beyond. *Ann. Phys.* **321**, 2–111 (2006).
39. H. Yao, S. A. Kivelson, Exact chiral spin liquid with non-abelian anyons. *Phys. Rev. Lett.* **99**, 247203 (2007).
40. Y. Ran, M. Hermele, P. A. Lee, X. G. Wen, Projected-wave-function study of the spin-1/2 Heisenberg model on the Kagomé lattice. *Phys. Rev. Lett.* **98**, 117205 (2007).
41. G. Jackeli, G. Khaliullin, Mott insulators in the strong spin-orbit coupling limit: From Heisenberg to a quantum compass and Kitaev models. *Phys. Rev. Lett.* **102**, 017205 (2009).
42. H. Yao, D. H. Lee, Fermionic magnons, non-abelian spinons, and the spin quantum hall effect from an exactly solvable spin-1/2 Kitaev model with $SU(2)$ symmetry. *Phys. Rev. Lett.* **107**, 087205 (2011).
43. S. V. Isakov, M. B. Hastings, R. G. Melko, Topological entanglement entropy of a Bose-Hubbard spin liquid. *Nat. Phys.* **7**, 772–775 (2011).
44. S. Yan, D. A. Huse, S. R. White, Spin-liquid ground state of the $s = 1/2$ Kagome Heisenberg antiferromagnet. *Science* **332**, 1173–1176 (2011).
45. P. Corboz, M. Lajkó, A. M. Läuchli, K. Penc, F. Mila, Spin-orbital quantum liquid on the honeycomb lattice. *Phys. Rev. X* **2**, 041013 (2012).
46. S. Depenbrock, I. P. McCulloch, U. Schollwöck, Nature of the spin-liquid ground state of the $s = 1/2$ Heisenberg model on the Kagome lattice. *Phys. Rev. Lett.* **109**, 067201 (2012).
47. H. C. Jiang, H. Yao, L. Balents, Spin liquid ground state of the spin-$\frac{1}{2}$ square J_1-J_2 Heisenberg model. *Phys. Rev. B* **86**, 024424 (2012).
48. H. C. Jiang, Z. Wang, L. Balents, Identifying topological order by entanglement entropy. *Nat. Phys.* **8**, 902–905 (2012).
49. H. Yao, S. A. Kivelson, Exact spin liquid ground states of the quantum dimer model on the square and honeycomb lattices. *Phys. Rev. Lett.* **108**, 247206 (2012).
50. L. Wang, D. Poilblanc, Z. C. Gu, X. G. Wen, F. Verstraete, Constructing a gapless spin-liquid state for the spin-1/2 $J_1 - J_2$ heisenberg model on a square lattice. *Phys. Rev. Lett.* **111**, 037202 (2013).
51. R. V. Mishmash, J. R. Garrison, S. Bieri, C. Xu, Theory of a competitive spin liquid state for weak Mott insulators on the triangular lattice. *Phys. Rev. Lett.* **111**, 157203 (2013).
52. Y. C. He, D. N. Sheng, Y. Chen, Chiral spin liquid in a frustrated anisotropic Kagome Heisenberg model. *Phys. Rev. Lett.* **112**, 137202 (2014).
53. J. G. Rau, E. K. H. Lee, H. Y. Kee, Generic spin model for the honeycomb iridates beyond the Kitaev limit. *Phys. Rev. Lett.* **112**, 077204 (2014).
54. S. S. Gong, W. Zhu, L. Balents, D. N. Sheng, Global phase diagram of competing ordered and quantum spin-liquid phases on the Kagome lattice. *Phys. Rev. B* **91**, 075112 (2015).
55. H. J. Liao *et al*., Gapless spin-liquid ground state in the $s = 1/2$ Kagome antiferromagnet. *Phys. Rev. Lett.* **118**, 137202 (2017).
56. Y. C. He, M. P. Zaletel, M. Oshikawa, F. Pollmann, Signatures of Dirac cones in a DMRG study of the Kagome Heisenberg model. *Phys. Rev. X* **7**, 031020 (2017).
57. Y. C. Wang, X. F. Zhang, F. Pollmann, M. Cheng, Z. Y. Meng, Quantum spin liquid with even ising gauge field structure on Kagome lattice. *Phys. Rev. Lett.* **121**, 057202 (2018).
58. W. Zhu, X. Chen, Y. C. He, W. Witczak-Krempa, Entanglement signatures of emergent Dirac fermions: Kagome spin liquid and quantum criticality. *Sci. Adv.* **4**, eaat5535 (2018).
59. X. Y. Song, C. Wang, A. Vishwanath, Y. C. He, Unifying description of competing orders in two-dimensional quantum magnets. *Nat. Commun.* **10**, 4254 (2019).
60. S. Hu, W. Zhu, S. Eggert, Y. C. He, Dirac spin liquid on the spin-1/2 triangular Heisenberg antiferromagnet. *Phys. Rev. Lett.* **123**, 207203 (2019).
61. A. Szasz, J. Motruk, M. P. Zaletel, J. E. Moore, Chiral spin liquid phase of the triangular lattice Hubbard model: A density matrix renormalization group study. *Phys. Rev. X* **10**, 021042 (2020).
62. B. B. Chen *et al*., Quantum spin liquid with emergent chiral order in the triangular-lattice Hubbard model. *Phys. Rev. B* **106**, 094420 (2022).
63. H. K. Jin, R. Y. Sun, H. H. Tu, Y. Zhou, Unveiling a critical stripy state in the triangular-lattice $SU(4)$ spin-orbital model. *Sci. Bull.* **67**, 918–923 (2022).
64. W. Y. Liu *et al*., Emergence of gapless quantum spin liquid from deconfined quantum critical point. *Phys. Rev. X* **12**, 031039 (2022).
65. Y. F. Jiang, H. C. Jiang, Nature of quantum spin liquids of the $s = \frac{1}{2}$ Heisenberg antiferromagnet on the triangular lattice: A parallel DMRG study. *Phys. Rev. B* **107**, L140411 (2023).
66. X. J. Yu, S. H. Shi, L. Xu, Z. X. Li, Emergence of competing orders and possible quantum spin liquid in $SU(n)$ fermions. *Phys. Rev. Lett.* **132**, 036704 (2024).
67. Z. Han, S. A. Kivelson, Resonating valence bond states in an electron-phonon system. *Phys. Rev. Lett.* **130**, 186404 (2023).
68. Z. Han, S. A. Kivelson, Emergent gauge fields in band insulators. *Proc. Natl. Acad. Sci. U.S.A.* **122**, e2421778122 (2025).
69. X. Cai, Z. X. Li, H. Yao, Antiferromagnetism induced by bond Su-Schrieffer-Heeger electron-phonon coupling: A quantum Monte Carlo study. *Phys. Rev. Lett.* **127**, 247203 (2021).
70. X. Cai, Z. X. Li, H. Yao, Robustness of antiferromagnetism in the Su-Schrieffer-Heeger Hubbard model. *Phys. Rev. B* **106**, L081115 (2022).
71. A. Götz, S. Beyl, M. Hohenadler, F. F. Assaad, Valence-bond solid to antiferromagnet transition in the two-dimensional Su-Schrieffer-Heeger model by Langevin dynamics. *Phys. Rev. B* **105**, 085151 (2022).
72. C. Feng, B. Xing, D. Poletti, R. Scalettar, G. Batrouni, Phase diagram of the Su-Schrieffer-Heeger-Hubbard model on a square lattice. *Phys. Rev. B* **106**, L081114 (2022).
73. A. Götz, M. Hohenadler, F. F. Assaad, Phases and exotic phase transitions of a two-dimensional Su-Schrieffer-Heeger model. *Phys. Rev. B* **109**, 195154 (2024).
74. M. Troyer, U. J. Wiese, Computational complexity and fundamental limitations to fermionic quantum Monte Carlo simulations. *Phys. Rev. Lett.* **94**, 170201 (2005).
75. C. Wu, S. C. Zhang, Sufficient condition for absence of the sign problem in the fermionic quantum Monte Carlo algorithm. *Phys. Rev. B* **71**, 155115 (2005).
76. E. Berg, M. A. Metlitski, S. Sachdev, Sign-problem–free quantum Monte Carlo of the onset of antiferromagnetism in metals. *Science* **338**, 1606–1609 (2012).
77. Z. X. Li, Y. F. Jiang, H. Yao, Solving the fermion sign problem in quantum Monte Carlo simulations by majorana representation. *Phys. Rev. B* **91**, 241117 (2015).

78. Z. X. Li, Y. F. Jiang, H. Yao, Majorana-time-reversal symmetries: A fundamental principle for sign-problem-free quantum Monte Carlo simulations. *Phys. Rev. Lett.* **117**, 267002 (2016).
79. Z. C. Wei, C. Wu, Y. Li, S. Zhang, T. Xiang, Majorana positivity and the fermion sign problem of quantum Monte Carlo simulations. *Phys. Rev. Lett.* **116**, 250601 (2016).
80. R. Blankenbecler, D. J. Scalapino, R. L. Sugar, Monte Carlo calculations of coupled boson-fermion systems. I. *Phys. Rev. D* **24**, 2278–2286 (1981).
81. J. E. Hirsch, Two-dimensional Hubbard model: Numerical simulation study. *Phys. Rev. B* **31**, 4403–4419 (1985).
82. F. Assaad, H. Evertz, *World-Line and Determinantal Quantum Monte Carlo Methods for Spins, Phonons and Electrons*, H. Fehske, R. Schneider, A. Weiße, Eds. (Springer, Berlin Heidelberg, Berlin, Heidelberg, 2008), pp. 277–356.
83. J. Gubernatis, N. Kawashima, P. Werner, *Quantum Monte Carlo Methods* (Cambridge University Press, 2016).
84. T. Senthil, M. P. A. Fisher, Z_2 gauge theory of electron fractionalization in strongly correlated systems. *Phys. Rev. B* **62**, 7850–7881 (2000).
85. A. Tanjaroon Ly, B. Cohen-Stead, S. Malkaruge Costa, S. Johnston, Comparative study of the superconductivity in the Holstein and optical Su-Schrieffer-Heeger models. *Phys. Rev. B* **108**, 184501 (2023).
86. M. Feldbacher, F. F. Assaad, Efficient calculation of imaginary-time-displaced correlation functions in the projector auxiliary-field quantum Monte Carlo algorithm. *Phys. Rev. B* **63**, 073105 (2001).
87. E. Lieb, T. Schultz, D. Mattis, Two soluble models of an antiferromagnetic chain. *Ann. Phys.* **16**, 407–466 (1961).
88. M. Oshikawa, Topological approach to Luttinger's theorem and the fermi surface of a Kondo lattice. *Phys. Rev. Lett.* **84**, 3370–3373 (2000).
89. M. B. Hastings, Lieb-Schultz-Mattis in higher dimensions. *Phys. Rev. B* **69**, 104431 (2004).
90. S. Kivelson, Statistics of holons in the quantum hard-core dimer gas. *Phys. Rev. B* **39**, 259–264 (1989).
91. D. Arovas, J. R. Schrieffer, F. Wilczek, Fractional statistics and the quantum hall effect. *Phys. Rev. Lett.* **53**, 722–723 (1984).
92. S. V. Isakov, R. G. Melko, M. B. Hastings, Universal signatures of fractionalized quantum critical points. *Science* **335**, 193–195 (2012).
93. J. Yu *et al*., Non-trivial quantum geometry and the strength of electron-phonon coupling. *Nat. Phys.* **20**, 1262–1268 (2024).
94. H. C. Jiang, S. A. Kivelson, High temperature superconductivity in a lightly doped quantum spin liquid. *Phys. Rev. Lett.* **127**, 097002 (2021).
95. Z. X. Li, S. G. Louie, D. H. Lee, Emergent superconductivity and non-fermi liquid transport in a doped valence bond solid insulator. *Phys. Rev. B* **107**, L041103 (2023).
96. Y. F. Jiang, H. C. Jiang, Topological superconductivity in the doped chiral spin liquid on the triangular lattice. *Phys. Rev. Lett.* **125**, 157002 (2020).
97. Y. F. Jiang, H. Yao, F. Yang, Possible superconductivity with a Bogoliubov Fermi surface in a lightly doped Kagome u(1) spin liquid. *Phys. Rev. Lett.* **127**, 187003 (2021).
98. C. Peng, Y. F. Jiang, D. N. Sheng, H. C. Jiang, Doping quantum spin liquids on the Kagome lattice. *Adv. Quantum Technol.* **4**, 2000126 (2021).